

Scintillation of pseudo-Bessel correlated beams in atmospheric turbulence

Yalong Gu and Greg Gbur

Department of Physics and Optical Science, University of North Carolina at Charlotte, Charlotte, North Carolina 28223, USA

Received June 14, 2010; revised October 20, 2010; accepted October 22, 2010;
posted October 22, 2010 (Doc. ID 130167); published November 17, 2010

The concept of pseudo-Bessel correlated beams is introduced, and their scintillation properties on propagation through turbulence are investigated. By using the Rytov approximation, the scintillation index of pseudo-Bessel correlated beams is formulated in weak turbulence. The study of scintillation is extended into strong turbulence by numeric simulations. It is shown that by choosing an appropriate coherence parameter, pseudo-Bessel correlated beams have lower scintillation than comparable fully coherent beams in both weak and strong turbulence. In addition, the configuration of pseudo-Bessel correlated beams is modified by adding a horizontal beamlet; the scintillation properties of these modified beams are also discussed. © 2010 Optical Society of America

OCIS codes: 010.1300, 030.0030.

1. INTRODUCTION

It is well known that optical beams are distorted on propagation through atmospheric turbulence, resulting in scintillation, beam wander, beam spreading, and decrease of spatial coherence [1]. In particular, the presence of scintillations—intensity fluctuations arising from the turbulence-induced random phase modulation—is especially problematic and is one of the fundamental limitations in the development of free-space optical communication systems [2].

In the past several decades, a large amount of work has been done on the scintillation properties of optical beams in random media. It is now well appreciated that the scintillation of a partially coherent beam or partially coherent multiple beams can be lower than that of its fully coherent counterpart [3–9]. On propagation through turbulence, a partially coherent beam delivers its energy through multiple incoherent spatial modes, each of which has its own distinct propagation path and intensity pattern. Because of mutual independence of these modes, the intensity of the complete partially coherent beam is the superposition of the individual intensity patterns, and on average the intensity received by the detector is more uniform. Recently a wave optics simulation approach of partially coherent beams was developed [10] and applied in the study of their propagation in turbulence [11,12].

So far, most studies on the propagation of partially coherent beams in turbulence have focused on the beams whose spatial correlation function is Gaussian. It has been shown that the scintillation reduction by a Gaussian correlated beam is negligible in the strong turbulence regime ([1], Chap. 16). However, other beam types have unusual propagation properties. Bessel beams, also referred to as nondiffracting beams, have an invariant field distribution across any plane orthogonal to the direction of propagation [13,14]. They are also shown to be able to reconstruct their initial intensity profiles after both ampli-

tude and phase perturbations [15,16]. The counterparts of Bessel beams in the partially coherent regime are Bessel correlated beams [17]. It has been demonstrated that a Bessel correlated beam of infinite size is propagation-invariant in free space and in *ABCD* systems [18,19], while a Bessel correlated beam of Gaussian intensity profile remains almost invariant up to a certain propagation distance [20]. It is also known that Bessel correlated beams can be used in focal spot shaping [21]. On noting the unusual properties of Bessel correlated beams in free-space propagation, it is natural to consider their scintillation properties when propagating in turbulence.

Although an elegant modal expansion of Bessel correlated beams was described in [17], it is still relatively difficult to mathematically formulate the scintillation of Bessel correlated beams on propagation in turbulence. In this paper, we introduce the concept of pseudo-Bessel correlated beams by using a discretized form of the Bessel correlation function. A pseudo-Bessel correlated beam is synthesized by the incoherent superposition of a collection of beamlets whose wave vectors form a cone. When the number of constituent beamlets approaches infinity, the field takes on the form of a Bessel correlated beam. The scintillation properties of pseudo-Bessel correlated beams of Gaussian intensity profile are investigated analytically and numerically. It is shown that with the appropriate coherence parameter, pseudo-Bessel correlated beams have lower scintillation than fully coherent beams of the same initial intensity profile in both weak and strong turbulence. It is also found that the maximum scintillation reduction can be obtained by a pseudo-Bessel correlated beam with a finite number of constituent beamlets. These results suggest that beam arrays generally perform comparably to or better than continuous partially coherent beams in scintillation reduction. In addition, the configuration of pseudo-Bessel correlated beams is modified by adding a horizontal beamlet. The addi-

tional beamlet keeps the scintillation of the modified pseudo-Bessel correlated beams at a low level for a relatively large range of the correlation length.

2. MODEL OF PSEUDO-BESSEL CORRELATED BEAMS

The second-order coherence properties of a wavefield in the source plane $z=0$ can be characterized by the cross-spectral density [22]

$$W(\boldsymbol{\rho}_1, \boldsymbol{\rho}_2, \omega) = \langle U(\boldsymbol{\rho}_1, \omega)U^*(\boldsymbol{\rho}_2, \omega) \rangle, \quad (1)$$

where $\boldsymbol{\rho}_1$ and $\boldsymbol{\rho}_2$ are the position vectors in the source plane, and $U(\boldsymbol{\rho}, \omega)$ is a realization of the wavefield at position $\boldsymbol{\rho}$ with angular frequency ω . Here angle brackets denote the average over an ensemble of monochromatic realizations of the field. The cross-spectral density may always be written as

$$W(\boldsymbol{\rho}_1, \boldsymbol{\rho}_2, \omega) = \sqrt{S(\boldsymbol{\rho}_1, \omega)}\sqrt{S(\boldsymbol{\rho}_2, \omega)}\mu(\boldsymbol{\rho}_1, \boldsymbol{\rho}_2, \omega), \quad (2)$$

where $S(\boldsymbol{\rho}, \omega) = W(\boldsymbol{\rho}, \boldsymbol{\rho}, \omega)$ is the spectral density at $\boldsymbol{\rho}$, and $\mu(\boldsymbol{\rho}_1, \boldsymbol{\rho}_2, \omega)$ is the spectral degree of coherence of the field at $\boldsymbol{\rho}_1$ and $\boldsymbol{\rho}_2$, whose absolute value is restricted to the range between 0 and 1. The extreme value zero represents spatial incoherence and the value unity represents complete spatial coherence at frequency ω . From now on we will focus on a single frequency ω and suppress its depiction in the function arguments. For a Bessel correlated beam, its spectral degree of coherence takes on the form

$$\mu(\boldsymbol{\rho}_1, \boldsymbol{\rho}_2) = J_0\left(\frac{|\boldsymbol{\rho}_1 - \boldsymbol{\rho}_2|}{r_0}\right), \quad (3)$$

where J_0 is the zeroth-order Bessel function of the first kind, and r_0 is the effective correlation length.

When investigating the properties of a partially coherent beam, one important issue is the synthesis of the wavefield such that its cross-spectral density is of a given form. For a Bessel correlated beam characterized by Eq. (3), we note that a Bessel function satisfies the well-known identity ([23], Chap. 11)

$$J_0\left(\frac{|\boldsymbol{\rho}_1 - \boldsymbol{\rho}_2|}{r_0}\right) = \frac{1}{2\pi} \int_0^{2\pi} \exp[ik\mathbf{u}_\perp \cdot (\boldsymbol{\rho}_1 - \boldsymbol{\rho}_2)] d\varphi_{u_\perp}, \quad (4)$$

where k is wavenumber, $|\mathbf{u}_\perp| = 1/(kr_0)$, and φ_{u_\perp} is the azimuthal angle of \mathbf{u}_\perp . On substituting Eq. (4) into Eq. (2) and discretizing the integral, the cross-spectral density can be approximated by a finite number of modes as

$$W(\boldsymbol{\rho}_1, \boldsymbol{\rho}_2) \approx \sum_{n=1}^N A_n(\boldsymbol{\rho}_1)A_n^*(\boldsymbol{\rho}_2), \quad (5)$$

where

$$A_n(\boldsymbol{\rho}) = \frac{1}{\sqrt{N}} \sqrt{S(\boldsymbol{\rho})} \exp(ik\mathbf{u}_{\perp n} \cdot \boldsymbol{\rho}), \quad (6)$$

N is the number of modes, and $\mathbf{u}_{\perp n} = (1/kr_0, 2n\pi/N)$ in polar coordinates. It can be seen that a Bessel correlated beam can be synthesized by the beamlets specified by Eq. (6) when N approaches infinity. As shown by Fig. 1, the wave vectors of these beamlets form a cone whose vertex

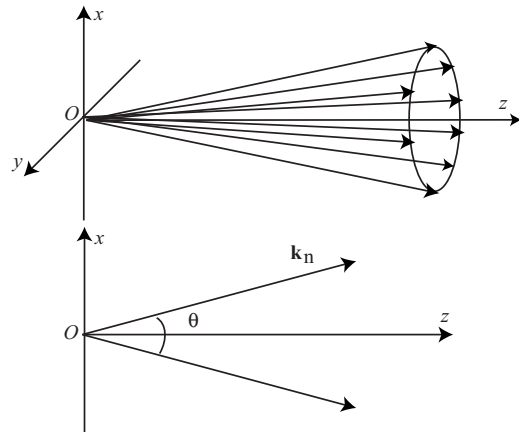


Fig. 1. Configuration of a pseudo-Bessel correlated beam. \mathbf{k}_n is the wave vector of the n th beamlet. $\mathbf{k}_n = k\mathbf{u}_n$, and its direction is specified by the unit vector \mathbf{u}_n whose projection in the source plane is $\mathbf{u}_{\perp n}$. $\theta = 2 \arcsin(|\mathbf{u}_{\perp n}|)$ is the vertex of cone.

angle is inversely related to the correlation length r_0 . When N is of finite value, we define a partially coherent beam whose cross-spectral density is specified by Eqs. (5) and (6) as a pseudo-Bessel correlated beam. Figure 1 also illustrates a potential method to generate a pseudo-Bessel correlated beam, i.e., a bundle of fiber lasers arranged either to directly diverge at angle θ or first converge in a source plane of angle θ .

It is to be noted that the scintillation of beam arrays has been considered before [24–26]. However such arrays consisted of beamlets spatially separated in the source plane, namely, spatially diverse arrays. The pseudo-Bessel correlated beams are directionally diverse beam arrays whose beamlets propagate in different directions.

In principle the spectral density $S(\rho)$ can be of arbitrary profile. In this paper, it is taken to be Gaussian, which is

$$S(\boldsymbol{\rho}) = \exp\left(-\frac{2\rho^2}{w_0^2}\right), \quad (7)$$

where w_0 indicates the width of the Gaussian profile. The average intensity in the source plane $L=0$ is therefore a Gaussian, regardless of state of coherence.

3. FORMULATION OF SCINTILLATION INDEX IN WEAK TURBULENCE

We consider a pseudo-Bessel correlated beam whose constituent beamlets are specified by Eqs. (6) and (7) at the source plane $z=0$. On propagation through weak turbulence, the wavefield of the n th beamlet can be represented by a so-called Rytov series [1],

$$A_n(\boldsymbol{\rho}, z) = A_{0n}(\boldsymbol{\rho}, z) \exp[\psi_{n1}(\boldsymbol{\rho}, z) + \psi_{n2}(\boldsymbol{\rho}, z) + \dots], \quad (8)$$

where $A_{0n}(\boldsymbol{\rho}, z)$ is the wavefield of the n th beamlet in the absence of the turbulence, and $\psi_{n1}(\boldsymbol{\rho}, z)$ and $\psi_{n2}(\boldsymbol{\rho}, z)$ are the complex phase perturbations of the first and the second order associated with the n th beamlet, respectively. With the assumption of weak turbulence, perturbation terms of order higher than two are neglected.

Because of the mutual independence of the constituent beamlets, the intensity of the pseudo-Bessel correlated beam at the receiver plane $z=L$ is

$$I(\boldsymbol{\rho}, L) = \sum_{n=1}^N I_n(\boldsymbol{\rho}, L), \quad (9)$$

where $I_n(\boldsymbol{\rho}, L) = |A_n(\boldsymbol{\rho}, L)|^2$ is the intensity of the n th beamlet. The intensity fluctuations of the pseudo-Bessel correlated beam at the receiver plane are characterized by the scintillation index which is defined as

$$\sigma^2(\boldsymbol{\rho}, L) = \frac{\langle I^2(\boldsymbol{\rho}, L) \rangle}{\langle I(\boldsymbol{\rho}, L) \rangle^2} - 1, \quad (10)$$

where the angle brackets stand for the average of the realizations of turbulence. With Eq. (9), the scintillation index can be rewritten as

$$\sigma^2(\boldsymbol{\rho}, L) = \frac{\sum_{m=1}^N \sum_{n=1}^N \langle I_m(\boldsymbol{\rho}, L) I_n(\boldsymbol{\rho}, L) \rangle}{\left(\sum_{n=1}^N \langle I_n(\boldsymbol{\rho}, L) \rangle \right)^2} - 1. \quad (11)$$

Within the framework of the Rytov approximation, the average intensity of the n th beamlet $\langle I_n(\boldsymbol{\rho}, L) \rangle$ and the average cross-intensity between the m th and n th beamlets $\langle I_m(\boldsymbol{\rho}, L) I_n(\boldsymbol{\rho}, L) \rangle$ in Eq. (11) are formulated by (for the detailed derivations, see Appendix A)

$$\langle I_n(\boldsymbol{\rho}, L) \rangle = |A_{0n}(\boldsymbol{\rho}, L)|^2 \exp\{2 \operatorname{Re}[E_1^n(\boldsymbol{\rho}, L)] + E_2^{nn}(\boldsymbol{\rho}, L)\}, \quad (12)$$

$$\langle I_m(\boldsymbol{\rho}, L) I_n(\boldsymbol{\rho}, L) \rangle = \langle I_m(\boldsymbol{\rho}, L) \rangle \langle I_n(\boldsymbol{\rho}, L) \rangle \times \exp\{2 \operatorname{Re}[E_2^{mn}(\boldsymbol{\rho}, L)] + 2 \operatorname{Re}[E_3^{mn}(\boldsymbol{\rho}, L)]\}, \quad (13)$$

where

$$\begin{aligned} E_1^n(\boldsymbol{\rho}, L) &= -\pi k^2 \exp\left[\frac{ikLu_{\perp n}^2}{2p(L)}\right] \int \Phi_n(\boldsymbol{\kappa}) d^2\boldsymbol{\kappa} \\ &\times \int_0^L \exp\left[\frac{-ik\eta u_{\perp n}^2}{2p(\eta)}\right] \\ &\times \exp\left[\frac{-ik\gamma(\eta)(L-\eta)u_{\perp n}^2}{2p^2(\eta)}\right] d\eta, \end{aligned} \quad (14)$$

$$\begin{aligned} E_2^{mn}(\boldsymbol{\rho}, L) &= 2\pi k^2 \exp\left[\frac{ikLu_{\perp m}^2}{2p(L)}\right] \exp\left[\frac{-ikLu_{\perp n}^2}{2p^*(L)}\right] \\ &\times \int_0^L \exp\left\{\frac{-ik}{2p(\eta)}\left[\eta + \frac{\gamma(\eta)(L-\eta)}{p(\eta)}\right]u_{\perp m}^2\right\} \\ &\times \exp\left\{\frac{ik}{2p^*(\eta)}\left[\eta + \frac{\gamma^*(\eta)(L-\eta)}{p^*(\eta)}\right]u_{\perp n}^2\right\} d\eta \\ &\times \int \exp\left\{\frac{-i[\gamma(\eta) - \gamma^*(\eta)](L-\eta)\boldsymbol{\kappa}^2}{2k}\right\} \end{aligned}$$

$$\begin{aligned} &\times \exp\{i[\gamma(\eta) - \gamma^*(\eta)]\boldsymbol{\kappa} \cdot \boldsymbol{\rho}\} \times \exp\left\{-i(L\right. \\ &\left. - \eta)\boldsymbol{\kappa} \cdot \left[\frac{\mathbf{u}_{\perp m}}{p(L)} - \frac{\mathbf{u}_{\perp n}}{p^*(L)}\right]\right\} \Phi_n(\boldsymbol{\kappa}) d^2\boldsymbol{\kappa}, \end{aligned} \quad (15)$$

$$\begin{aligned} E_3^{mn}(\boldsymbol{\rho}, L) &= -2\pi k^2 \exp\left[\frac{ikLu_{\perp m}^2}{2p(L)}\right] \exp\left[\frac{ikLu_{\perp n}^2}{2p(L)}\right] \\ &\times \int_0^L \exp\left\{\frac{-ik}{2p(\eta)}\left[\eta + \frac{\gamma(\eta)(L-\eta)}{p(\eta)}\right](u_{\perp m}^2\right. \\ &\left. + u_{\perp n}^2)\right\} d\eta \int \exp\left[\frac{-i(L-\eta)}{p(L)}\boldsymbol{\kappa} \cdot (\mathbf{u}_{\perp m}\right. \\ &\left. - \mathbf{u}_{\perp n})\right] \exp\left[\frac{-i\gamma(\eta)(L-\eta)\boldsymbol{\kappa}^2}{k}\right] \Phi_n(\boldsymbol{\kappa}) d^2\boldsymbol{\kappa}, \end{aligned} \quad (16)$$

where $p(L) = 1 + i2L/kw_0^2$, $\gamma(\eta) = p(\eta)/p(L)$ and $\Phi_n(\boldsymbol{\kappa})$ is the power spectrum of the turbulence.

4. EXAMPLES AND ANALYSIS

In this paper, the turbulence is modeled by the von Karman spectrum

$$\Phi_n(\boldsymbol{\kappa}) = 0.033 C_n^2 \frac{\exp(-\boldsymbol{\kappa}^2/\kappa_m^2)}{(\boldsymbol{\kappa}^2 + \kappa_0^2)^{11/6}}, \quad (17)$$

where $\kappa_m = 5.92/l_m$ with the inner scale $l_m = 1$ mm and $\kappa_0 = 1/l_0$ with the outer scale $l_0 = 10$ m. The scintillation index of a pseudo-Bessel correlated beam can be numerically evaluated by substituting Eqs. (12)–(17) into Eq. (11).

Figure 2 shows the on-axis scintillation index of a pseudo-Bessel correlated beam as a function of the relative correlation length r_0/w_0 in weak turbulence when the number of constituent beamlets is two. The turbulence strength parameter is $C_n^2 = 10^{-15} \text{ m}^{-2/3}$, and the propagation distance is $L = 2$ km. The on-axis scintillation index of a fully coherent Gaussian beam with the same width w_0 is shown on the plot as a horizontal line for comparison. Its scintillation value can be also obtained by numerically evaluating the formulas developed in Section 3 when $N = 1$ and $\mathbf{u}_{\perp} = 0$. It can be seen that a minimum of the scintillation for a pseudo-Bessel correlated beam occurs when $r_0/w_0 \approx 0.32$, providing 50% reduction as compared to the scintillation of a Gaussian beam alone. The simulated on-axis scintillation indices of some different r_0/w_0 are also shown in Fig. 2 for comparison. We applied a multiple phase screen method for the simulations [27], in which extended turbulence is modeled by a collection of phase screens at appropriate distances and with carefully chosen statistical properties, and the field undergoes free-space propagation between them. The constituent beamlets given by Eq. (6) are propagated through the same realization of the turbulence, and their intensities are added at the receiver plane according to Eq. (9). The simulated scintillation values are obtained by the ensemble average of 2000 realizations. As shown by Fig. 2,

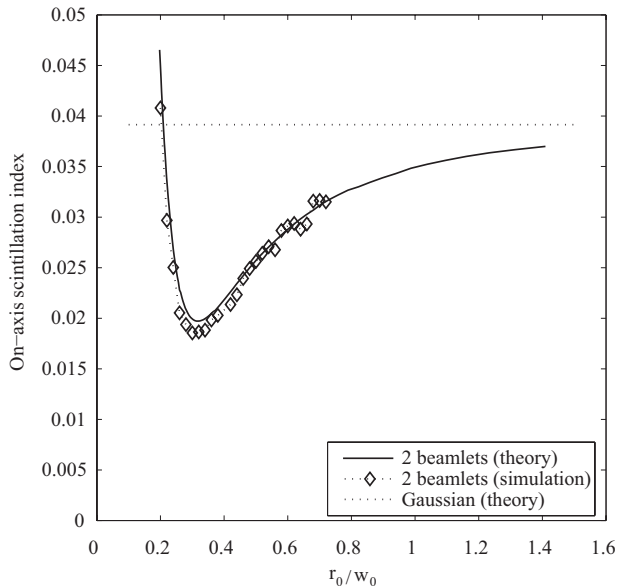


Fig. 2. On-axis scintillation of a 2-beamlet pseudo-Bessel correlated beam as a function of the relative correlation length r_0/w_0 . Here the wavelength is taken to be $\lambda=1.55\ \mu\text{m}$, and the width of the beam is taken to be $w_0=0.05\ \text{m}$. The turbulence strength parameter is $C_n^2=10^{-15}\ \text{m}^{-2/3}$ and the propagation distance is $L=2\ \text{km}$.

the numeric results have good agreement with the analytic results obtained by the Rytov theory.

The origin of the minimum scintillation can be understood as follows. In the high-coherence regime (large r_0), the constituent beamlets propagate near the horizontal axis and through nearly the same region of turbulence. The scintillation of the pseudo-Bessel correlated beam is approximately the same as the scintillation of the horizontal Gaussian beam. On the decrease of coherence, the spatial separation between the beamlets' propagation paths is enlarged. Their propagation through the turbulence is less correlated and on average the scintillation of the pseudo-Bessel correlated beam is reduced. However, in the low-coherence regime (small r_0), the propagation paths of the constituent beamlets are distant from the horizontal axis. The scintillation of the pseudo-Bessel correlated beam is increased because of the low intensity detected by the receiver. Therefore there exists an optimal correlation length for which the scintillation of the pseudo-Bessel correlated beam is minimum. Beams with different widths ranging from $w_0=3\ \text{cm}$ to $w_0=7\ \text{cm}$ were also studied; the qualitative features described here were present in all cases, though the optimal correlation length varies with beam size.

Figure 3 illustrates the dependence of the on-axis scintillation index of a pseudo-Bessel correlated beam on the number of its constituent beamlets. The relative correlation length r_0/w_0 is 0.33. As N increases, the on-axis scintillation index falls and saturates rapidly. When N is small, the propagation of the additional beamlets is still relatively uncorrelated with the propagation of the existing beamlets, and the scintillation of the pseudo-Bessel correlated beam is reduced. However, when N is large, the additional beamlets propagate through very similar regions of turbulence as the existing beamlets and make no

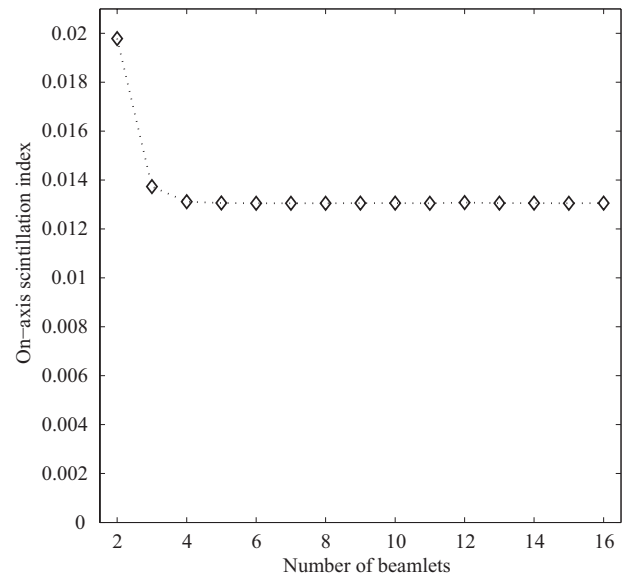


Fig. 3. On-axis scintillation of a pseudo-Bessel correlated beam as a function of the number of its constituent beamlets N . The relative correlation length is taken to be $r_0/w_0=0.33$. The rest of the parameters are the same as in Fig. 2.

contribution to the further scintillation reduction. From Fig. 3, it can be seen that the scintillation of a Bessel correlated beam can be studied through the scintillation of a pseudo-Bessel correlated beam with the finite number of constituent beamlets. As illustrated by Fig. 4, the maximum scintillation reduction is 79% when the number of constituent beamlets is 16. Significantly, this result suggests that the most significant scintillation reduction is achieved with a finite number of incoherent beamlets, and that familiar classes of partially coherent beams, such as Schell-model beams, are in a sense “wasteful.” A Schell-model beam can be decomposed using an angular spectrum representation into a sum of uncorrelated plane waves propagating in different directions [28]. Plane

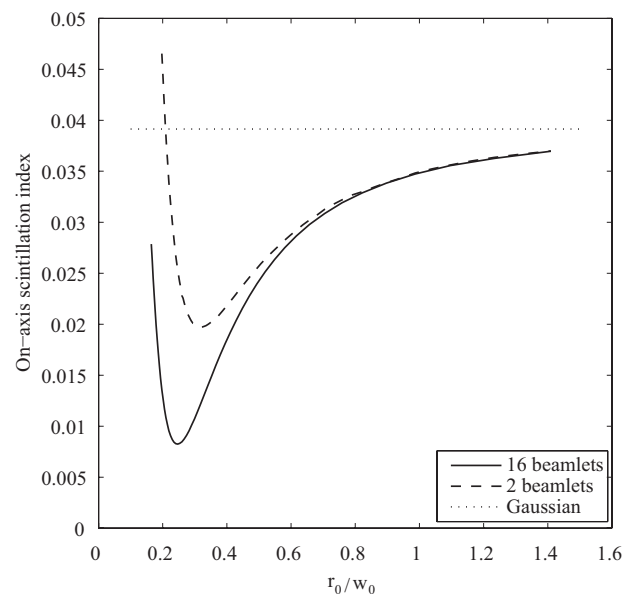


Fig. 4. On-axis scintillation of a 16-beamlet pseudo-Bessel correlated beam as a function of the relative correlation length r_0/w_0 . The parameters are the same as in Fig. 2.

waves propagating in very similar directions will be affected by turbulence in very much the same manner, and will not provide any significant reduction in scintillation.

The analytic formulas for scintillation of pseudo-Bessel correlated beams obtained by the Rytov approximation in Section 3 is valid only in weak turbulence. However the multiple phase screen simulation method applied in Fig. 2 retains its validity for Gaussian beams in the strong turbulence regime [29]. Now we extend the study on the scintillation of pseudo-Bessel correlated beams into the strong turbulence regime by numeric simulations. The turbulence strength parameter is $C_n^2 = 10^{-14} \text{ m}^{-2/3}$ and the propagation distance is $L = 3 \text{ km}$. As shown in Fig. 5, the similar behavior of on-axis scintillation index of a pseudo-Bessel correlated beam as a function of the relative correlation length r_0/w_0 is observed, and the maximum scintillation reduction saturates as the increase of the number of constituent beamlets N . When $N = 8$, 73.2% scintillation reduction is obtained when $r_0/w_0 = 0.28$. Figure 6 illustrates the on-axis scintillation index of an 8-beamlet pseudo-Bessel correlated beam as a function of the Rytov variance,

$$\sigma_1^2 = 1.23 C_n^2 k^{7/6} L^{11/6}. \quad (18)$$

The beam is of the optimal correlation length obtained from Fig. 5. It can be seen that the pseudo-Bessel correlated beam significantly outperforms the Gaussian beam.

It is to be noted that Figs. 2, 4, and 5 do not extend to $r_0/w_0 = 0$. In this limit, the beamlets are propagating perpendicular to the z axis and essentially no light intensity is reaching the detector. In this case, the scintillations get arbitrarily large, and we have excluded that limit from the plots for clarity.

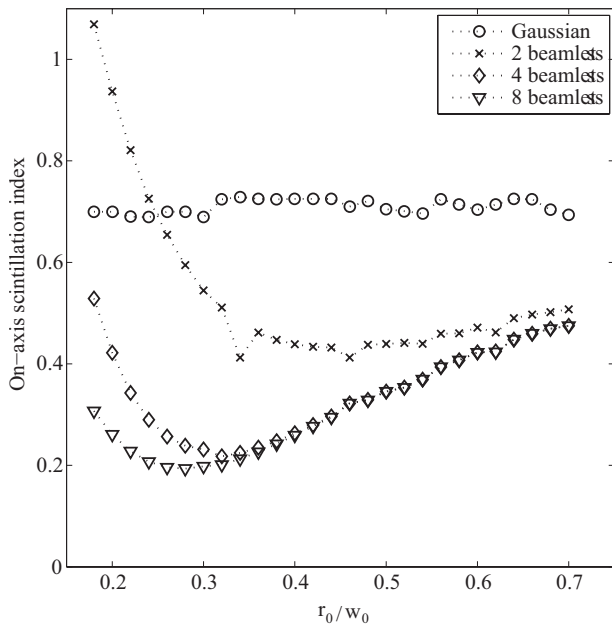


Fig. 5. On-axis scintillation of a pseudo-Bessel correlated beam as a function of the relative correlation length r_0/w_0 . The wavelength is also $\lambda = 1.55 \mu\text{m}$ and the width of the beam is $w_0 = 0.05 \text{ m}$. Here the turbulence strength parameter is $C_n^2 = 10^{-14} \text{ m}^{-2/3}$ and the propagation distance is $L = 3 \text{ km}$.

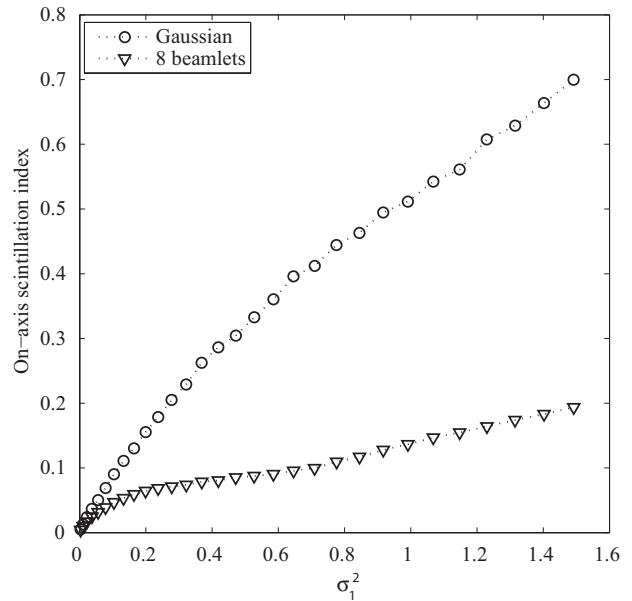


Fig. 6. On-axis scintillation of an 8-beamlet pseudo-Bessel correlated beam as a function of the Rytov variance $\sigma_1^2 = 1.23 C_n^2 k^{7/6} L^{11/6}$. The relative correlation length is $r_0/w_0 = 0.28$ and the other parameters are the same as in Fig. 5.

5. SCINTILLATION OF MODIFIED PSEUDO-BESSEL CORRELATED BEAMS

As discussed in Section 4, the scintillation of a pseudo-Bessel correlated beam increases rapidly if the correlation length decreases further after reaching its optimal value. This arises because the beamlets mostly “miss” the detector, but high variations in intensity are produced when a beamlet occasionally wanders into its range. To correct this, we modified the configuration of pseudo-Bessel correlated beams by adding an independent horizontal beamlet

$$E(\boldsymbol{\rho}, z = 0) = E_0 \exp\left(-\frac{\rho^2}{w_0^2}\right), \quad (19)$$

where E_0 is the amplitude. For simplicity, its beam width is also w_0 .

It can be shown that the on-axis scintillation index of the modified pseudo-Bessel correlated beam takes on the minimum value given by

$$\sigma_{min}^2 = \begin{cases} \frac{\sigma_{pb}^2 \sigma_h^2 - (\sigma_{pb,h}^2)^2}{\sigma_{pb}^2 + \sigma_h^2 - 2\sigma_{pb,h}^2} & \text{if } \sigma_{pb,h}^2 < \min[\sigma_{pb}^2, \sigma_h^2] \\ \min[\sigma_{pb}^2, \sigma_h^2] & \text{otherwise} \end{cases}, \quad (20)$$

when

$$E_0 = \sqrt{\frac{I_{pb}(\sigma_{pb}^2 - \sigma_{pb,h}^2)}{I_h(\sigma_h^2 - \sigma_{pb,h}^2)}} \quad \text{if } \sigma_{pb,h}^2 < \min[\sigma_{pb}^2, \sigma_h^2]. \quad (21)$$

In Eqs. (20) and (21), σ_{pb}^2 and σ_h^2 are the on-axis scintillation indices of the pseudo-Bessel correlated beam and the horizontal beamlet, respectively. $\sigma_{pb,h}^2$ is the on-axis cross scintillation index between the pseudo-Bessel correlated beam and the horizontal beamlet, which is defined as

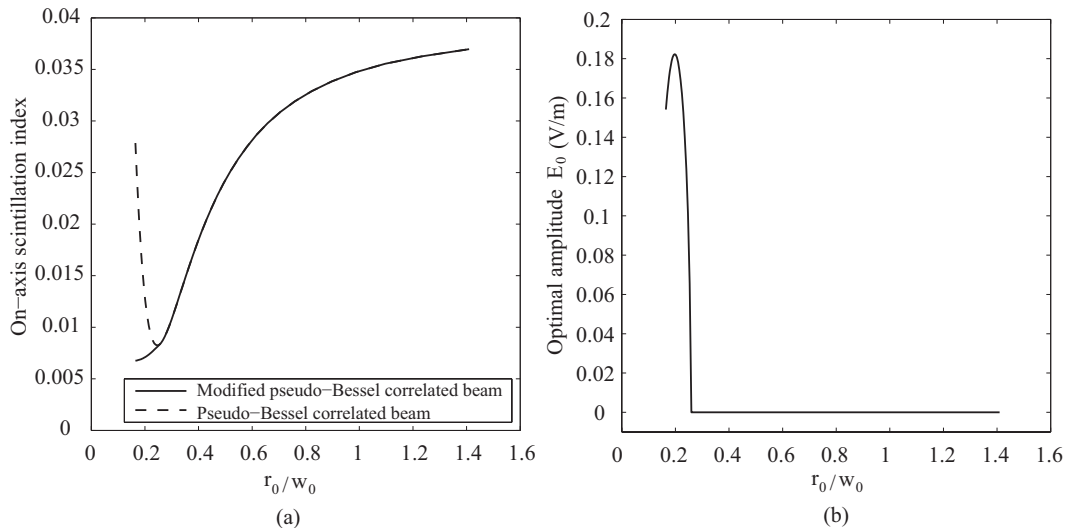


Fig. 7. (a) Dashed curve shows the on-axis scintillation of a 16-beamlet pseudo-Bessel correlated beam as a function of the relative correlation length r_0/w_0 , while the solid curve shows the minimum on-axis scintillation of the corresponding modified pseudo-Bessel correlated beam. The optimal amplitude E_0 is shown in (b). The parameters are the same as in Fig. 4.

$$\sigma_{pb,h}^2 = \frac{\langle I_{pb} I_h \rangle}{\langle I_{pb} \rangle \langle I_h \rangle} - 1. \tag{22}$$

I_{pb} and I_h are the on-axis intensities of the pseudo-Bessel correlated beam and the horizontal beamlet. The factor $\min[\sigma_{pb}^2, \sigma_h^2]$ takes the minimum between σ_{pb}^2 and σ_h^2 . In addition, with the assumption of isotropic turbulence, it can be shown that $\sigma_{pb,h}^2 = \sigma_{n,h}^2$, where

$$\sigma_{n,h}^2 = \frac{\langle I_n I_h \rangle}{\langle I_n \rangle \langle I_h \rangle} - 1 \tag{23}$$

is the on-axis cross scintillation index between the n th beamlet of the pseudo-Bessel correlated beam and the horizontal beamlet.

In weak turbulence, the minimum on-axis scintillation index of the modified pseudo-Bessel correlated beams [Eq.

(20)] can be numerically evaluated by the formulas driven in Section 3. It is illustrated as a function of the relative correlation length r_0/w_0 in Fig. 7. The corresponding optimal amplitude E_0 is also shown. The number of constituent beamlets of the pseudo-Bessel correlated beam is 16. It can be seen that when coherence is relatively high, the minimum on-axis scintillation index of the modified pseudo-Bessel correlated beam is the on-axis scintillation index of the pseudo-Bessel correlated beam itself because $\sigma_{pb}^2 < \sigma_{pb,h}^2$ and $\sigma_{pb}^2 < \sigma_h^2$. Therefore there is no need to add the additional horizontal beamlet in this regime. However in the low-coherence regime, $\sigma_{pb,h}^2 < \min[\sigma_{pb}^2, \sigma_h^2]$, the additional horizontal beamlet keeps the scintillation of the modified pseudo-Bessel correlated beams at a low level for a relatively large range of the correlation length r_0 . If r_0 further decreases, we can anticipate that the detected on-axis intensity is dominated by the additional horizontal

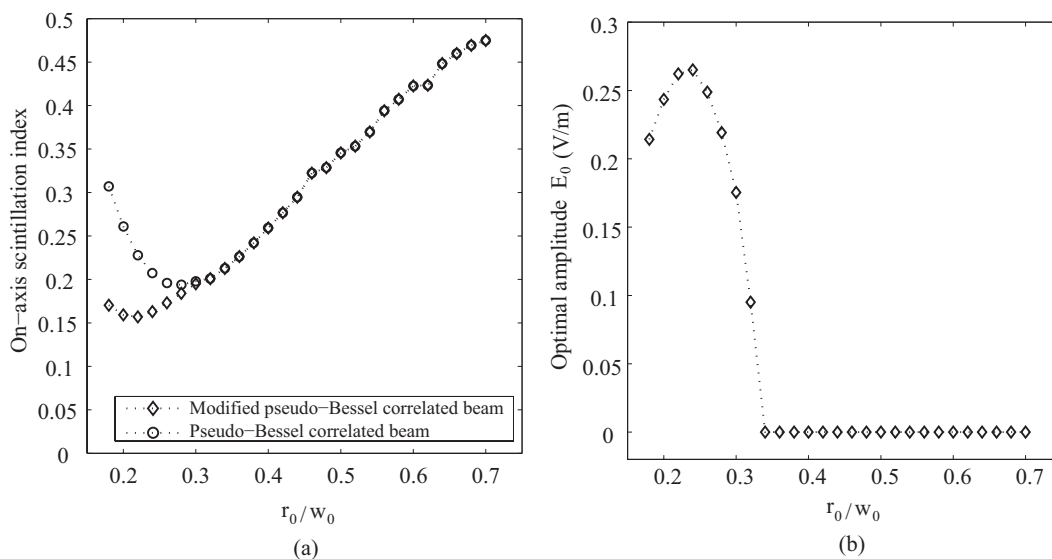


Fig. 8. (a) Dashed curve shows the on-axis scintillation of an 8-beamlet pseudo-Bessel correlated beam as a function of the relative correlation length r_0/w_0 , while the solid curve shows the minimum on-axis scintillation of the corresponding modified pseudo-Bessel correlated beam. The optimal amplitude E_0 is shown in (b). The parameters are the same as in Fig. 5.

beamlet, and the on-axis scintillation index of the modified pseudo-Bessel correlated beam increases and approaches σ_n^2 eventually.

Figure 8 illustrates the minimum on-axis scintillation index of the modified pseudo-Bessel correlated beams as well as the optimal amplitude E_0 in strong turbulence; these quantities are obtained by numeric simulations. The number of constituent beams of the pseudo-Bessel correlated beam is eight. A behavior similar to that of Fig. 7 is observed.

6. CONCLUSIONS

We have investigated the scintillation properties of pseudo-Bessel correlated beams of Gaussian intensity profile in both weak and strong turbulence. With an appropriately chosen coherence parameter, it is demonstrated that such beams have lower scintillation than comparable fully coherent Gaussian beams.

It is noted that the scintillation rapidly decreases to an asymptotic limit as the number of beamlets is increased. This suggests that, in general, the optimal scintillation reduction can always be achieved with a relatively small and finite number of such beamlets, and that partially coherent fields with more complicated coherence properties will not provide significant improvement.

We have also studied the scintillation properties of pseudo-Bessel correlated beams combined with a central horizontal beamlet. The additional beamlet keeps the scintillation of the so-called modified pseudo-Bessel correlated beams at a low level for a relatively wide range of values of the correlation length r_0 .

Although the spectral density $S(\boldsymbol{\rho})$ is chosen to be Gaussian, the synthesis method of Bessel correlation applied in this paper can be used to study the propagation of Bessel correlated beams of other intensity profiles through the atmosphere. For instance, the constituent beamlets could be taken to be of nonuniform polarization [30], or of Bessel–Gaussian form [28,31].

APPENDIX A: DERIVATION OF E_1^n , E_2^{mn} , AND E_3^{mn}

In this Appendix, we derive the expressions for E_1^n , E_2^{mn} , and E_3^{mn} given above [Eqs. (14)–(16)]. They are the second-order statistical moments, which are defined as

$$E_1^n(\boldsymbol{\rho}, L) = \langle \psi_{n2}(\boldsymbol{\rho}, L) \rangle + \frac{1}{2} \langle \psi_{n1}(\boldsymbol{\rho}, L) \rangle^2, \quad (\text{A1})$$

$$E_2^{mn}(\boldsymbol{\rho}, L) = \langle \psi_{m1}(\boldsymbol{\rho}, L) \psi_{n1}^*(\boldsymbol{\rho}, L) \rangle, \quad (\text{A2})$$

$$E_3^{mn}(\boldsymbol{\rho}, L) = \langle \psi_{m1}(\boldsymbol{\rho}, L) \psi_{n1}(\boldsymbol{\rho}, L) \rangle. \quad (\text{A3})$$

The expressions for the average intensity $\langle I_n(\boldsymbol{\rho}, L) \rangle$ [Eq. (12)] and the average cross-intensity $\langle I_m(\boldsymbol{\rho}, L) I_n(\boldsymbol{\rho}, L) \rangle$ [Eq. (13)] can be obtained by the similar derivations as shown in [1] and [24], respectively.

By the Rytov approximation, the wavefield in the turbulence can be expressed by Eq. (8). For the n th beamlet specified by Eqs. (6) and (7), it can be shown that by using

the angular spectrum theory the wavefield at the receiver plane $z=L$ in the absence of the turbulence is

$$A_{0n}(\boldsymbol{\rho}, L) = \frac{1}{\sqrt{Np(L)}} \exp \left[ikL - \frac{\rho^2}{p(L)w_0^2} \right] \exp \left[\frac{i(2k\mathbf{u}_{\perp n} \cdot \boldsymbol{\rho} - kLu_{\perp n}^2)}{2p(L)} \right]. \quad (\text{A4})$$

The first-order complex phase perturbation term $\psi_{n1}(\boldsymbol{\rho}, L)$ can be evaluated by the following equation [[1], Chap. 5, Eq. (36)]

$$\psi_{n1}(\boldsymbol{\rho}, L) = \frac{k^2}{2\pi} \int_0^L dz \int \exp \left[ik(L-z) + \frac{ik|\mathbf{s} - \boldsymbol{\rho}|^2}{2(L-z)} \right] \frac{A_{0n}(\mathbf{s}, z) n_1(\mathbf{s}, z)}{A_{0n}(\boldsymbol{\rho}, L) L-z} d^2s. \quad (\text{A5})$$

$n_1(\boldsymbol{\rho}, z)$ is the turbulence-induced refractive index fluctuation, which can be written in the following form:

$$n_1(\boldsymbol{\rho}, z) = \iint \exp(i\boldsymbol{\kappa} \cdot \boldsymbol{\rho}) dv(\boldsymbol{\kappa}, z), \quad (\text{A6})$$

where $dv(\boldsymbol{\kappa}, z)$ is the random amplitude of $n_1(\boldsymbol{\rho}, z)$. On substituting Eqs. (A4) and (A6) into Eq. (A5), we arrive at [after integrating with respect to the variable \mathbf{s}]

$$\begin{aligned} \psi_{n1}(\boldsymbol{\rho}, L) &= ik \exp \left[\frac{ikLu_{\perp n}^2}{2p(L)} \right] \\ &\times \int_0^L \exp \left\{ \frac{-ik}{2p(z)} \left[z + \frac{\gamma(z)(L-z)}{p(z)} \right] u_{\perp n}^2 \right\} dz \\ &\times \iint \exp \left[-\frac{i\gamma(z)(L-z)\kappa^2}{2k} \right] \exp[i\gamma(z)\boldsymbol{\kappa} \cdot \boldsymbol{\rho}] \\ &\times \exp \left[-\frac{i\gamma(z)(L-z)}{p(z)} \boldsymbol{\kappa} \cdot \mathbf{u}_{\perp n} \right] dv(\boldsymbol{\kappa}, z), \end{aligned} \quad (\text{A7})$$

where again $\gamma(z) = p(z)/p(L)$. E_2^{mn} can be obtained by substituting Eq. (A7) into Eq. (A2). With the relationship

$$\langle dv(\boldsymbol{\kappa}, z) dv^*(\boldsymbol{\kappa}', z') \rangle = F_n(\boldsymbol{\kappa}, |z-z'|) \delta(\boldsymbol{\kappa} - \boldsymbol{\kappa}') d^2\kappa d^2\kappa', \quad (\text{A8})$$

where δ is the Dirac delta function and $F_n(\boldsymbol{\kappa}, |z-z'|)$ is a two dimensional spectral density of the turbulence, we have, after some calculations,

$$\begin{aligned} E_2^{mn}(\boldsymbol{\rho}, L) &= k^2 \exp \left[\frac{ikLu_{\perp m}^2}{2p(L)} \right] \exp \left[\frac{-ikLu_{\perp n}^2}{2p^*(L)} \right] \\ &\times \int_0^L \int_0^L \exp \left\{ \frac{-ik}{2p(z)} \left[z + \frac{\gamma(z)(L-z)}{p(z)} \right] u_{\perp m}^2 \right\} \\ &\times \exp \left\{ \frac{ik}{2p^*(z')} \left[z' + \frac{\gamma^*(z')(L-z')}{p^*(z')} \right] u_{\perp n}^2 \right\} dz dz' \end{aligned}$$

$$\begin{aligned} & \times \int \int \exp \left\{ -\frac{i}{2k} [\gamma(z)(L-z) - \gamma^*(z')] \right. \\ & \times (L-z') \kappa^2 \left. \exp \left\{ -i\boldsymbol{\kappa} \cdot \left[\frac{L-z}{p(L)} \mathbf{u}_{\perp m} \right. \right. \right. \\ & \left. \left. \left. - \frac{L-z'}{p^*(L)} \mathbf{u}_{\perp n} \right] \right\} \exp [i\gamma(z) \right. \\ & \left. - \gamma^*(z')] \boldsymbol{\kappa} \cdot \boldsymbol{\rho} \right\} F_n(\boldsymbol{\kappa}, |z-z'|) d^2\boldsymbol{\kappa}. \end{aligned} \quad (\text{A9})$$

Now we replace the integration variables z and z' by $\eta = (z+z')/2$ and $\mu = z-z'$. With the assumption that the turbulence is delta correlated in the propagation direction, $F_n(\boldsymbol{\kappa}, \mu)$ has appreciable values only when $\mu \approx 0$. Thus we can extend the integration on μ from $-\infty$ to ∞ without significant error and let $z \approx z' \approx \eta$. With these approximations and the relationship between $F_n(\boldsymbol{\kappa}, \mu)$ and the power spectrum of the turbulence $\Phi_n(\boldsymbol{\kappa})$,

$$\Phi_n(\boldsymbol{\kappa}) = \frac{1}{2\pi} \int_{-\infty}^{\infty} F_n(\boldsymbol{\kappa}, \mu) d\mu, \quad (\text{A10})$$

Eq. (A9) can reduce to the expression

$$\begin{aligned} E_2^{mn}(\boldsymbol{\rho}, L) &= 2\pi k^2 \exp \left[\frac{ikLu_{\perp m}^2}{2p(L)} \right] \exp \left[\frac{-ikLu_{\perp n}^2}{2p^*(L)} \right] \\ & \times \int_0^L \exp \left\{ \frac{-ik}{2p(\eta)} \left[\eta + \frac{\gamma(\eta)(L-\eta)}{p(\eta)} \right] u_{\perp m}^2 \right\} \\ & \times \exp \left\{ \frac{ik}{2p^*(\eta)} \left[\eta + \frac{\gamma^*(\eta)(L-\eta)}{p^*(\eta)} \right] u_{\perp n}^2 \right\} d\eta \\ & \times \int \exp \left\{ \frac{-i[\gamma(\eta) - \gamma^*(\eta)](L-\eta)\kappa^2}{2k} \right\} \\ & \times \exp \left\{ i[\gamma(\eta) - \gamma^*(\eta)] \boldsymbol{\kappa} \cdot \boldsymbol{\rho} \right\} \exp \left\{ -i(L \right. \\ & \left. - \eta) \boldsymbol{\kappa} \cdot \left[\frac{\mathbf{u}_{\perp m}}{p(L)} - \frac{\mathbf{u}_{\perp n}}{p^*(L)} \right] \right\} \Phi_n(\boldsymbol{\kappa}) d^2\boldsymbol{\kappa}, \end{aligned} \quad (\text{A11})$$

which is Eq. (15) for E_2^{mn} . Equation (16) for E_3^{mn} can be obtained by a similar derivation, except that the following relationship is used:

$$\langle dv(\boldsymbol{\kappa}, z) dv(\boldsymbol{\kappa}', z') \rangle = F_n(\boldsymbol{\kappa}, |z-z'|) \delta(\boldsymbol{\kappa} + \boldsymbol{\kappa}') d^2\boldsymbol{\kappa} d^2\boldsymbol{\kappa}'. \quad (\text{A12})$$

For E_1^n defined as Eq. (A1), it has been shown that it is equivalent to the ensemble average of the second-order normalized Born perturbation term [[1], Chap. 5, Eqs. (35) and (39)]. Therefore, it can be derived by using the following equation [[1], Chap. 5, Eq. (40)]:

$$\begin{aligned} E_1^n(\boldsymbol{\rho}, L) &= \frac{k^2}{2\pi} \int_0^L dz \int \exp \left[ik(L-z) + \frac{ik|\mathbf{s}-\boldsymbol{\rho}|^2}{2(L-z)} \right] \\ & \times \frac{A_{0n}(\mathbf{s}, z) \langle \psi_{n1}(\mathbf{s}, z) n_1(\mathbf{s}, z) \rangle}{A_{0n}(\boldsymbol{\rho}, L) L-z} d^2\mathbf{s}. \end{aligned} \quad (\text{A13})$$

On substituting Eqs. (A4), (A6), and (A7) into Eq. (A13),

we have, after integrating with respect to the variable \mathbf{s} ,

$$\begin{aligned} E_1^n(\boldsymbol{\rho}, L) &= -k^2 \exp \left[\frac{ikLu_{\perp n}^2}{2p(L)} \right] \int_0^L dz \int_0^z dz' \exp \left\{ -\frac{ik}{2} \left[\frac{z'}{p(z')} \right. \right. \\ & \left. \left. + \frac{\gamma'(z-z')}{p^2(z')} + \frac{\gamma(L-z)}{p^2(z)} \right] u_{\perp n}^2 \right\} \\ & \times \int \int \int \int_{-\infty}^{\infty} \langle dv(\boldsymbol{\kappa}, z) dv(\boldsymbol{\kappa}', z') \rangle \\ & \times \exp \left[-\frac{i\gamma'(z-z')\kappa'^2}{2k} \right] \\ & \times \exp \left[-\frac{i\gamma'(z-z')}{p(z')} \boldsymbol{\kappa}' \cdot \mathbf{u}_{\perp n} \right] \\ & \times \exp \left[-\frac{i\gamma(L-z)|\boldsymbol{\kappa} + \gamma'\boldsymbol{\kappa}'|^2}{2k} \right] \exp \left[-\frac{i\gamma(L-z)}{p(z)} \right. \\ & \left. \times (\boldsymbol{\kappa} + \gamma'\boldsymbol{\kappa}') \cdot \mathbf{u}_{\perp n} \right] \exp [i\gamma(\boldsymbol{\kappa} + \gamma'\boldsymbol{\kappa}') \cdot \boldsymbol{\rho}], \end{aligned} \quad (\text{A14})$$

where $\gamma = p(z)/p(L)$ and $\gamma' = p(z')/p(z)$. Equation (A14) can be simplified by using the relationship Eq. (A12) and the similar approximations as applied in the derivation of E_2^{mn} . Recognizing that $\gamma' \approx 1$ and the integration on μ is from 0 and ∞ , it can reduce to

$$\begin{aligned} E_1^n(\boldsymbol{\rho}, L) &= -\pi k^2 \exp \left[\frac{ikLu_{\perp n}^2}{2p(L)} \right] \int \Phi_n(\boldsymbol{\kappa}) d^2\boldsymbol{\kappa} \\ & \times \int_0^L \exp \left[\frac{-ik\eta u_{\perp n}^2}{2p(\eta)} \right] \\ & \times \exp \left[\frac{-ik\gamma(\eta)(L-\eta)u_{\perp n}^2}{2p^2(\eta)} \right] d\eta, \end{aligned} \quad (\text{A15})$$

which is Eq. (14).

ACKNOWLEDGMENTS

This research was supported by the U. S. Air Force Office of Scientific Research (AFOSR) under grant FA9550-08-1-0063.

REFERENCES

1. L. C. Andrews and R. L. Phillips, *Laser Beam Propagation through Random Media*, 2nd ed. (SPIE Press, 2005).
2. L. C. Andrews, R. L. Phillips, and C. Y. Hopen, *Laser Beam Scintillation with Applications* (SPIE Press, 2001).
3. J. C. Leader, "Intensity fluctuations resulting from partially coherent light propagating through atmospheric turbulence," *J. Opt. Soc. Am.* **69**, 73–83 (1979).
4. V. A. Banakh, V. M. Buldakov, and V. L. Mironov, "Intensity fluctuations of a partially coherent light beam in a turbulent atmosphere," *Opt. Spectrosc.* **54**, 1054–1059 (1983).
5. Y. Baykal, M. A. Plonus, and S. J. Wang, "The scintillations for weak atmospheric turbulence using a partially coherent source," *Radio Sci.* **18**, 551–556 (1983).
6. J. C. Ricklin and F. M. Davidson, "Atmospheric turbulence effects on a partially coherent Gaussian Beam: implications for free-space laser communication," *J. Opt. Soc. Am. A* **19**,

- 1794–1802 (2002).
7. O. Korotkova, L. C. Andrews, and R. L. Phillips, “A model for a partially coherent Gaussian beam in atmospheric turbulence with application in lasercom,” *Opt. Eng.* **43**, 330–341 (2004).
 8. T. J. Schulz, “Optimal beams for propagation through random media,” *Opt. Lett.* **30**, 1093–1095 (2005).
 9. Y. Baykal, H. T. Eyyuboğlu, and Y. Cai, “Scintillations of partially coherent multiple Gaussian beams in turbulence,” *Appl. Opt.* **48**, 1943–1954 (2009).
 10. X. Xiao and D. Voelz, “Wave optics simulation approach of partially coherent beams,” *Opt. Express* **14**, 6986–6992 (2006).
 11. X. Xiao and D. Voelz, “On-axis probability density function and fade behavior of partially coherent beams propagating through turbulence,” *Appl. Opt.* **48**, 167–175 (2009).
 12. X. Qian, W. Zhu, and R. Rao, “Numerical investigation on propagation effects of pseudo-partially coherent Gaussian-Schell model beams in atmospheric turbulence,” *Opt. Express* **17**, 3782–3791 (2009).
 13. J. Durnin, J. J. Miceli, Jr., and J. H. Eberly, “Diffraction-free beams,” *Phys. Rev. Lett.* **58**, 1499–1501 (1987).
 14. J. Durnin, “Exact solutions for nondiffracting beams. I. The scalar theory,” *J. Opt. Soc. Am. A* **4**, 651–654 (1987).
 15. Z. Bouchal, J. Wagner, and M. Chlup, “Self-reconstruction of a distorted nondiffracting beam,” *Opt. Commun.* **151**, 207–211 (1998).
 16. Z. Bouchal, “Resistance of nondiffracting vortex beam against amplitude and phase perturbations,” *Opt. Commun.* **210**, 155–164 (2002).
 17. F. Gori, G. Guattaria, and C. Padovani, “Modal expansion of J_0 -correlated Schell-model sources,” *Opt. Commun.* **64**, 311–316 (1987).
 18. J. Turunen, A. Vasara, and A. T. Friberg, “Propagation invariance and self-imaging in variable-coherence optics,” *J. Opt. Soc. Am. A* **8**, 282–289 (1991).
 19. A. T. Friberg, A. Vasara, and J. Turunen, “Partially coherent propagation-invariant beams: Passage through paraxial optical systems,” *Phys. Rev. A* **43**, 7079–7082 (1991).
 20. C. Palma, R. Borghi, and G. Cincotti, “Beams originated by J_0 -correlated Schell-model planar sources,” *Opt. Commun.* **125**, 113–121 (1996).
 21. G. Gbur and T. Visser, “Can spatial coherence effects produce a local minimum of intensity at focus?” *Opt. Lett.* **28**, 1627–1629 (2003).
 22. L. Mandel and E. Wolf, *Optical Coherence and Quantum Optics* (Cambridge University Press, 1995).
 23. G. B. Arfken and H. J. Weber, *Mathematical Methods for Physicists*, 4th ed. (Academic, 1995).
 24. A. Peleg and J. V. Moloney, “Scintillation index for two Gaussian laser beams with different wavelengths in weak atmospheric turbulence,” *J. Opt. Soc. Am. A* **23**, 3114–3122 (2006).
 25. P. Polynkin, A. Peleg, L. Klein, T. Rhoadarmer, and J. V. Moloney, “Optimized multi-emitter beams for free-space optical communications through turbulent atmosphere,” *Opt. Lett.* **32**, 885–887 (2007).
 26. A. Peleg and J. V. Moloney, “Scintillation reduction by use of multiple Gaussian laser beams with different wavelengths,” *IEEE Photonics Technol. Lett.* **19**, 883–885 (2007).
 27. J. M. Martin and S. M. Flatté, “Intensity images and statistics from numerical simulation of wave propagation in 3-D random media,” *Appl. Opt.* **27**, 2111–2126 (1988).
 28. G. Gbur and O. Korotkova, “Angular spectrum representation for the propagation of arbitrary coherent and partially coherent beams through atmospheric turbulence,” *J. Opt. Soc. Am. A* **24**, 745–752 (2007).
 29. A. Belmonte, “Feasibility study for the simulation of beam propagation: consideration of coherent lidar performance,” *Appl. Opt.* **39**, 5426–5445 (2000).
 30. Y. Gu, O. Korotkova, and G. Gbur, “Scintillation of nonuniformly polarized beams in atmospheric turbulence,” *Opt. Lett.* **34**, 2261–2263 (2009).
 31. H. T. Eyyuboğlu, E. Sermutlu, Y. Baykal, Y. Cai, and O. Korotkova, “Intensity fluctuation in J -Bessel-Gaussian beams of all orders propagating in turbulent atmosphere,” *Appl. Phys. B: Lasers Opt.* **93**, 605–611 (2008).